Available online at www.sciencedirect.com
SCIENCE DIRECT®
Carbohydrate Research 338 (2003) 625–635
CARBOHYDRATE RESEARCH
www.elsevier.com/locate/carres

Macrocycle conformation and self-inclusion phenomena in octakis(3-*O*-butanoyl-2,6-di-*O*-pentyl)-γ-cyclodextrin (Lipodex E) by NMR spectroscopy and molecular dynamics

Andrea Mele,[a,*] Giuseppina Raffaini,[a] Fabio Ganazzoli,[a] Markus Juza,[b,†] Volker Schurig[c]

[a]*Dipartimento di Chimica, Materiali ed Ingegneria Chimica 'G. Natta'-Politecnico di Milano, Via L. Mancinelli 7, I-20131 Milano, Italy*
[b]*Laboratorium für Technische Chemie, ETH Hönggerberg, CH-8093 Zürich, Switzerland*
[c]*Institut of Organic Chemistry, University Tübingen, Auf der Morgenstelle 18, D-72076 Tübingen, Germany*

Received 18 September 2002; accepted 15 November 2002

Abstract

Octakis(3-*O*-butanoyl-2,6-di-*O*-pentyl)-γ-cyclodextrin (Lipodex E) is a lipophilic chiral selector successfully used for the enantioselective gas chromatographic separation of a multitude of racemic analytes. NMR data (^{13}C chemical shifts, $^{3}J_{HH}$, rotating frame NOEs (ROEs)) and molecular dynamics (MD) simulations point out that the macrocycle is distorted with respect to the canonical truncated-cone shape of native cyclodextrins, although C_8 symmetry is retained on the NMR timescale. ROE data and MD trajectories provide evidence for self-inclusion of one 6-*O*-pentyl pendant chain within the cavity of Lipodex E. The interpretation of long-range and low-intensity ROEs is supported by the calculation of average internuclear distances by using the radial distribution function (RDF) calculated from MD trajectories. MD simulations are eventually used to compare the flexibility of the macrocycle of Lipodex E with that of native γCD.

Keywords: Cyclodextrins; Lipodex E; Molecular dynamics; NMR spectroscopy; Nuclear Overhauser effect; Radial distribution function

1. Introduction

Octakis(3-*O*-butanoyl-2,6-di-*O*-pentyl)-γ-cyclodextrin (Lipodex E, **1**, see Fig. 1) is a lipophilic derivative of γ-cyclodextrin (γCD) synthesized by chemical functionalization of the macrocycle.[1,2] It has been used as chiral stationary phase (CSP) for the separation of a large number of racemic analytes by analytical gas chromatography (GC).[3] Successful applications of **1** were also reported for preparative GC[4] and simulated moving bed (SMB) gas chromatography.[5]

The well-documented ability of chemically modified cyclodextrins to act as CSPs for enantioselective separations, especially by gas chromatography,[6] prompted many scientists to investigate the physical basis of molecular recognition and chiral discrimination when a vapour-phase mixture of analytes interacts with CSPs. However, the prediction of the retention behaviour of different classes of chiral analytes with given chiral selectors still remains a difficult task,[7–9] as detailed information on the selectand–selector interactions at the atomic level and on the sites of interaction are required. The formation of diastereomeric inclusion complexes between cyclodextrins and chiral analytes is the most frequently reported mechanism of chiral discrimination in GC and HPLC.[10] Nevertheless, in some cases multiple enantioselective retention mechanisms for the separation of chiral compounds have been proposed according to the fact that analytes can also interact with the external surface of CDs, thus forming two different kind of host–guest complexes: a genuine inclusion complex and/or a less specific, non-inclusion association with the derivatized glucose units.[11–13]

* Corresponding author. Tel.: +39-02-23993006; fax: +39-02-23993080
E-mail address: andrea.mele@polimi.it (A. Mele).
† Present address: CarboGen Laboratories (Aarau) AG, Schachenallee 29, CH-5001 Aarau, Switzerland.

0008-6215/03/$ - see front matter
PII: S0008-6215(02)00493-7

Recent results based on molecular dynamics (MD) simulations indicated that the major contribution to the host–guest binding and enantiomer discrimination is due to the inclusion of the analyte into the CD cavity. Binding to the external surface of the host seems to be a minor component either to the strength of the host–guest association or the enantioselectivity, but it becomes increasingly important as the polarity of the analytes increases.[14–18] Knowledge of the conformational preferences of the receptor (compound **1** in the present case) is a pivotal prerequisite for understanding its ability to interact with the selectand and the recognition process. The role played by the macrocycle geometry in the molecular-recognition process was recently stressed for synthetic cyclooligosaccharides, such as α-cycloaltrin.[19] In that case, the 'induced-fit'[20] mechanism, rather than 'lock and key' type,[21] was demonstrated to drive the host ability to include guest molecules.

The extensive chemical derivatization of γCD in **1** is expected to alter the conformation of the glucose units and of the macrocycle with respect to the native γCD, hence allowing for different mechanisms of host–guest interaction. Moreover, the possibility of self-inclusion of one (or possibly more) of the 24 alkyl and acyl side chains into the CD cavity has to be taken into account as a factor potentially affecting the mechanism of host–guest association. To this end, a thorough experimental and theoretical investigation of the conformation of **1**, mainly focused onto the macrocycle and alkyl/acyl chains properties, is reported in the present work, and the results of one- and two-dimensional NMR experiments and of MD simulations are compared in detail.

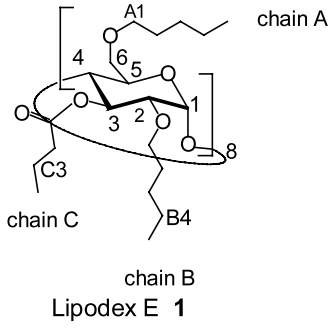

Fig. 1. Molecular structure and atom labelling of compound **1**. Carbohydrate atoms are indicated with the usual numbering. The *n*-th generic glucose unit is linked to the $(n-1)$-th unit via $\alpha(1\rightarrow4)$ glycosidic bond. For the description of NMR data the suffixes 'a' and 'b' indicate the diastereotopic protons of one methylene group resonating at higher and lower frequencies, respectively (e.g., H-6a and H-6b). Capital letters A, B and C indicate the acyl/alkyl side chains. Protons of side chains are labelled with the name of the chain followed by the carbon atom number (e.g., A1a means the proton attached to carbon 1 of chain A and resonating at higher frequency with respect to the geminal partner. The notation C-4 (hyphenated) indicates the carbon atom in position 4 of the glucopyranose ring, whilst C4 (not hyphenated) refers to all the protons attached to carbon 4 of side chain C). Some examples of side chains nomenclature and numbering (A1, B4 and C3) are given for the sake of clarity.

2. Results and discussion

2.1. NMR spectroscopy

The lipophilicity of **1** was exploited to perform an NMR study in water-free and low interacting cyclohexane-d_{12}. Under these conditions, the conformations assumed by **1** are expected to mimic, at an acceptable level of approximation, the interaction sites available to the selectand in the course of the gas-chromatographic process with the same CSP. The ^{1}H and ^{13}C NMR spectra of compound **1** showed a single set of signals, consistent with a retained C_8 symmetry of the γCD macrocycle on the NMR timescale. The full ^{1}H NMR characterization of **1** is summarised in Table 1. The values of the vicinal $^3J_{HH}$ coupling constants within the glucose backbone of **1** are consistent with the generally observed $^4C_1$ chair conformation of the glucose units of cyclodextrins on the NMR timescale.[22] For the sake of clarity, such $^3J_{HH}$ coupling constants are shown in Table 2, along with the literature values reported for native γCD[23] and for some chemically modified analogues, such as octakis(2,6-di-*O*-octyl)-γ-cyclodextrin (DO-γCD),[24] and per-*O*-methyl-γ-cyclodextrin (PM-γCD).[25] As the glucose units do not deviate from the $^4C_1$ chair conformation, the geometrical preferences of **1** are mainly driven by the conformation of the macrocycle and its side chains. The former is determined by the values of the torsion angles across the glycosidic linkage. It is known that the values of ^{13}C NMR chemical shift of carbon atoms involved in the glycosidic bridge, namely C-1 and C-4, are sensitive probes to changes in these torsion angles.[26] Recently, an investigation on large ring cyclodextrins (LR-CDs, 9 to 26 glucopyranose units) carried out with either X-ray crystallography or high-resolution ^{13}C NMR spectroscopy pointed out that variations of the chemical shift of C-1 and C-4 toward low frequency (shielding) are associated with new conformational motives of the macrocycle, which are different from canonical cone shapes.[27,28] The ^{13}C NMR data of compound **1** are reported in Table 3 along with literature data of the reference compounds mentioned above. A comparison of the chemical shift variations of C-2, C-3 and C-6 shows differences mainly driven by substituent effects (**1**, PM-γCD and DO-γCD versus native γCD). The chemical shift values observed for C-1 and C-4 of **1** are quite close to those of the homologous carbons of PM-γCD, proving that also **1** undergoes distortions from the cone shape of CDs. The presence of bulky substituents at-

Table 1
^{1}H NMR data [a] of compound **1** (500 MHz, cyclohexane-d_{12}, 305 K, external Me_4Si)

δ (ppm)	Integral, multiplicity and coupling constants (Hz)	Assignment
5.25	1 H, dd, J_{3-4} 8.9, J_{2-3} 9.8	H-3
5.03	1 H, d, J_{1-2} 3.5	H-1
3.92	1 H, dd, J_{6a-5} 3.5, $^2J_{6a-6b}$ −11.0	H-6a
3.81	1 H, m	H-5
3.72	1 H, dd, J_{3-4} 8.9, J_{4-5} 9.6	H-4
3.49	1 H, ddd, $J_1 = J_2$ 8.9, ^2J −9.2	B1a
3.42	1 H, ddd, $J_1 = J_2$ 6.3, ^2J −9.2	A1a
3.39	1 H, m	H-6b
3.32	1 H, ddd, $J_1 = J_2$ 6.3, ^2J −9.2	A1b
3.28	1 H, ddd, $J_1 = J_2$ 6.6, ^2J −9.2	B1b
3.13	1 H, dd, J_{1-2} 3.5, J_{2-3} 9.8	H-2
2.33	1 H, ddd, J_1 6.4, J_2 7.7, ^2J −15.7	C2a
2.06	1 H, ddd, $J_1 = J_2$ 7.4, ^2J −15.7	C2b
1.62–1.57	2 H, m	C3
1.54–1.41	4 H, m	A2 + B2
1.36–1.21	8 H, m	A3 + B3 + A4 + B4
0.864 [b]	3 H, t, J 7.3	C4
0.855	3 H, t, J 7.3	A5 or B5
0.853	3 H, t, J 7.3	B5 or A5

[a] See caption to Fig. 1 for proton labelling.
[b] The assignment of the methyl group C-4 was obtained by 1D-HOHAHA after selective excitation of C2a proton.

Table 2
Vicinal coupling constants ($^3J_{HH}$, Hz) of glucose protons of native γCD, some alkyl substituted γ-cyclodextrins and **1**

	J_{1-2}	J_{2-3}	J_{3-4}	J_{4-5}	J_{5-6a}	J_{5-6b}	J_{6a-6b}
γCD [a]	3.5	9.5	9.5	9.5	3.0	3.0	[e]
DO-γ-CD [b]	3.5	9.6	[e]	[e]	[e]	[e]	[e]
PM-γ-CD [c]	3.5	9.5	9.0	9.0	3.8	2.4	−10.5
1 [d]	3.5	9.8	8.9	9.6	3.1	[e]	−11.0

[a] In DMSO-d_6.[23]
[b] Octakis(2,6-di-*O*-octyl)-γ-cyclodextrin, $CDCl_3$, 298 K, reference Me_4Si. From Ref. 24.
[c] Permethyl-γ-cyclodextrin, D_2O. From Ref. 25.
[d] In cyclohexane-d_{12}, this work.
[e] Not reported or not determined.

tached to O-2, O-3 and O-6 of the γCD skeleton of **1** is expected to force the macrocycle to assume a non-symmetrical conformation in order to reduce steric strain.

Deeper insights into the conformational preferences of **1** were gained by 2D-ROESY experiments. Fig. 2 displays a detail of the contour plot of a ROESY experiment on **1**. The relative intensities of selected cross-peaks are reported in Table 4. The transverse NOE (ROE) data can be attributed to three contributions: intra-glucose, inter-glucose and glucose-alkyl/acyl chains transverse ROEs: (*i*) Intra-glucose ROEs. Due to the chemical derivatization, the chemical shift dispersion of **1** is larger than that normally observed in native CDs. This allows for the detection of a set of ROEs normally not achievable in native CDs due to peak overlap. The observed cross-peaks relating to H-2/H-4, H-3/H-5 and to H-1/H-2 pairs reflect the *syn*-1,3-diaxial and *syn*-1,2-equatorial-axial relationships, respectively, typical of $^4C_1$ α-D-glucopyranose units, thus confirming the presence of undistorted glucopyranose units in **1**, in agreement with the discussion on *J* couplings; (*ii*) inter-glucose ROEs. In native CDs the cross-relaxation between H-1 and H-4 of adjacent glucose units is the only inter-glucose (interglycosidic) contact usually detectable. In the presence of macrocycle deformation[29] associated to chemical functionalization at O-2, O-3 and O-6, the relative tilting of the glucose units is expected to yield inter-glucose NOEs usually not observed in native CDs, such as those involving H-1/H-5 and H-1/H-6.[30] The relative intensities of the cross peaks reported in Table 4 show appreciable H-1/H-5 and H-1/H-6a contacts. The latter is prevalently due to genuine dipolar contact, as no direct HOHAHA transfer is detectable either on H-4/H-6a or on H-5/H-6a proton pairs. The issue whether H-1/H-6a ROE peaks can be truly related to adjacent inter-glucose, rather than intra-glucose, dipolar contacts should be correctly addressed at this stage. To this end, MD simulations are useful since they allow a statistical determination of the distribution of the inter-nuclear distances via the radial distribution function (RDF) $g_{ij}(r)$. As detailed in Section 3 and here anticipated for clarity, this function yields the average density of probability of finding atoms *j* at a distance comprised between *r* and $r + dr$ from atoms *i*, irrespective of the direction of approach (in the following, the sets of atoms will be indicated in curly brackets as $\{i\}$ and $\{j\}$, and the *ij* subscript dropped for simplicity). Fig. 3 shows a comparison of $g(r)$ calculated over a 5-ns simulation for the distance between the {H-1} and {H-6} of **1** and native γCD (filled diamonds and empty circles, respectively). The maxima of the two curves match well for 4 Å $< r <$ 5 Å, indicating that the intra-glucose contribution to the overall distance distribution is comparable for the two cyclodextrins. Conversely, for $r < 4$ Å, i.e., the interesting internuclear distance range for NOE,[31] the main contribution is due to inter-glucose distances between $\{\text{H-1}(n)\}$ and $\{\text{H-6}(n-1)\}$. Here the two curves are markedly different. Native γCD shows a diffuse hump with a plateau for 3 Å $< r <$ 4 Å, meaning that all the distances within that interval have the same probability, whilst **1** shows a neat peak centred at 2.4 Å, associated with a well defined family of conformers. The H-1/H-6a ROE ob-

Table 3
^{13}C NMR chemical shifts (δ, ppm) of the glucose units carbon atoms of γCD, some alkyl substituted γ-cyclodextrins and **1**

CD\C atom	C-1	C-2	C-3	C-4	C-5	C-6
γ-CD [a]	104.26	74.91	75.53	83.02	74.37	62.82
DO-γ-CD [b]	101.8	80.8	73.3	83.2	70.4	69.1
PM-γ-CD [c]	98.29	82.92	83.19	76.74	72.12	73.40
1 [d]	97.64	79.64	72.56	76.33	72.29	70.50

[a] 125 MHz, D_2O, 298 K, reference external sodium 3-(trimethylsilyl) propane-1-sulfonate. From Ref. 23.
[b] Octakis(2,6-di-*O*-octyl)-γ-cyclodextrin. 100 MHz, $CDCl_3$, 298 K, reference Me_4Si. From Ref. 24.
[c] Permethyl-γ-cyclodextrin. 125 MHz, D_2O, 298 K, reference external sodium 3-(trimethylsilyl) propane-1-sulfonate. From Ref. 25.
[d] This work, 100 MHz, cyclohexane-d_{12}, 305 K, reference external Me_4Si.

served is thus consistent with the calculated interglycosidic distance frequencies and directly related to macrocycle distortions due to glucose tilting. On the other hand, the H-1/H-5 cross peak can be related to a two-step magnetization transfer: H-1 → H-4 (mediated by the inter-glucose ROE mentioned above), followed by intra-glucose H-4 → H-5 HOHAHA-type magnetization transfer (see Section 3). Such pathway for magnetization transfer affords 'false' rather than 'genuine' inter-glucose H-1/H-5 ROE.[31]; (*iii*) glucose–alkyl/acyl chain ROEs. Small, but significant, cross-peaks between some carbohydrate ring protons and some of the protons of the lipophilic side chains are also present (Table 4). This fact is remarkable, since it concerns also the glucose protons pointing toward the inner part of the cavity, H-3 and H-5 (see, for instance, the contacts of H-3 with the group of protons A3 + A4 + B3 + B4 or the methyl groups A5 + B5 + C4). These findings are consistent with the self-inclusion (intramolecular inclusion) of one of the lipophilic side chains into the cavity of **1**. Intermolecular inclusion, namely inclusion of one pentyl chain of a molecule into the cavity of an adjacent one, cannot be ruled out a priori. In principle, the alkyl chains of two adjacent molecules could interact favourably, thus leading to a loose association. However, the steric hindrance caused by these chains would prevent the deep insertion of one pentyl chain into the cavity of a second molecule of **1**. Thus, even in the presence of non-covalent dimeric or oligomeric association, the intermolecular inclusion would be a disadvantageous process. Moreover, the use of dilute solution (approx 5 mM) a fortiori made such a process unlikely to occur and mass spectrometric study carried out on **1** dissolved in cyclohexane gave a molecular weight consistent with monomeric **1** (see Section 3). Some examples of self-inclusion of apolar pendant groups of functionalized lipophilic cyclodextrins, typically aromatic ring systems,[32–37] are reported in the literature. Evidence for the self-inclusion is generally provided by the detection of glucose-pendant group ROEs. In the case of **1**, the ROEs observed between H-3 and the groups of protons (A3 + A4 + B3 + B4) and (A5 + B5 + C4) could be related to three different factors: (a) the direct interaction of H-3 with the chains B, as H-3 and the B alkyl chain are located in vicinal positions within the same glucopyranose ring; (b) the interaction of H-3 with the alkyl chain A via self-inclusion of the latter; (c) both these effects. Fig. 4 reports the RDF g(*r*) relating to the distribution of the distances of {H-3}, {H-4} and {H-5} with the hydrogen atoms of all the methyl groups {A5}. The portion of the curve for $r < 4$ Å is appreciably populated for {H-3} and {H-5}, showing that the observed H-3/(A5 + B5 + C4) ROE is consistent with self-inclusion of an A pentyl chain. Interestingly, the RDF g(*r*) for {H-4} points out that

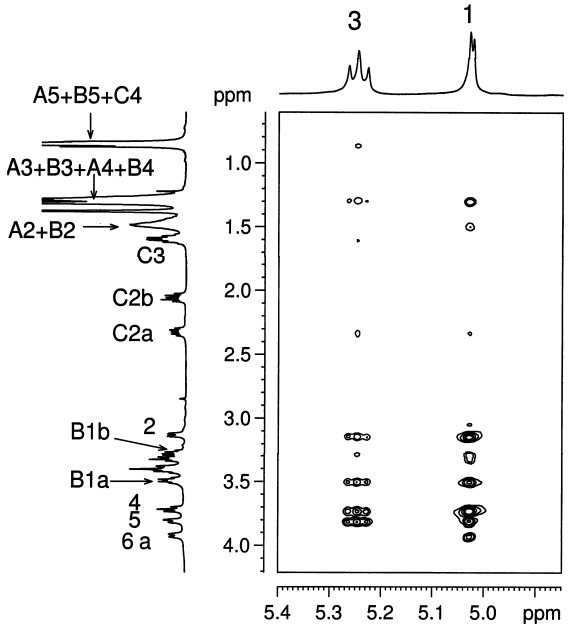

Fig. 2. Espansion of the contour plot of 2D-ROESY of **1**. The assignment of relevant protons is reported in the projections. Glucose rings protons are indicated with the position number without H (e.g., '3' or '6a' instead of 'H-3' or 'H-6a').

Table 4
Selection of relative cross-peaks intensities of ROESY experiment on **1** [a]

	H-1	H-2	H-3	H-4	H-5	H-6a	H-6b	A1a	A1b	B1a	B1b	C2a	C2b
H-1	[b]	2.18	0.17	2.74 [c]	0.86	0.52	0.00	0.00	0.19	0.95	0.32	0.11	[d]
H-2		[b]	0.45	0.80	0.22	0.00	0.00	0.00	0.00	0.58	1.19	0.00	0.00
H-3			[b]	0.68	1.00 [e]	0.00	0.00	0.00	0.00	0.47	0.33	0.23	0.13
H-4				[b]	[f]	0.30	0.67	[g]	0.00	0.00	0.00	0.00	0.00
H-5					[b]	0.31	1.61	[g]	0.0	0.00	0.00	0.00	0.00
H-6a						[b]	4.33	[g]	0.51				
C3	[c]		0.15							[d]	0.12		
A2+B2	0.20	0.20	0.17	0.18	0.15	[d]							
A3+A4+B3+B4	0.33	0.18	0.29	0.29	0.24	[d]							
A5+B5+C4	[c]	0.11	0.15	[d]	[d]								

[a] All the cross-peaks volumes are normalized to H-3/H-5 cross peak volume. The values not essential for the discussion or already reported as symmetrical cross-peak (e.g., H-1/H-5 and H-5/H-1) correspond to empty cells of the table.
[b] Diagonal peak.
[c] Interglycosidic.
[d] Less than 0.1.
[e] Reference value arbitrarily set to 1.00.
[f] Cross-peak due to HOHAHA magnetization transfer (in phase with diagonal).
[g] Not determined due to peak overlap.

these protons are not in the distance range for the detection of ROE with {A5}. This provides a rationale for the interpretation of the observed H-4/(A3 + A4 + B3 + B4) cross peak (Table 4): it may be entirely due to interaction of H-4 with chain B only or to 'false' ROE due to H-5/H-4 HOHAHA transfer.

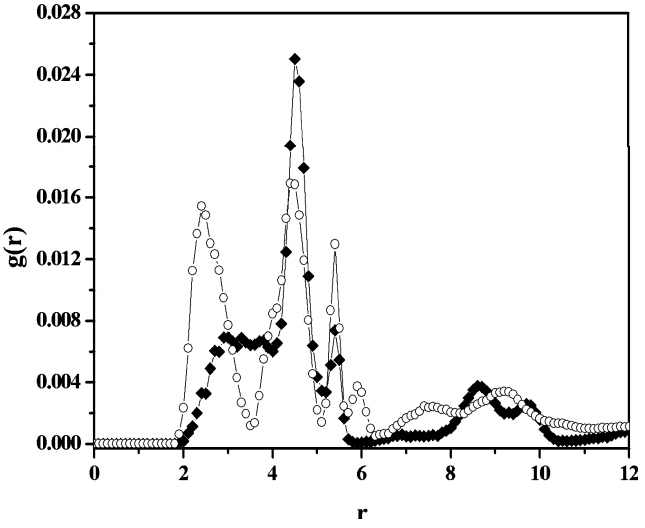

Fig. 3. Spherical radial distribution function $g(r)$ of the {H-1}–{H-6} distance r (Å) in **1** (empty circles) and native γCD (filled diamonds) calculated over 5 ns MD simulation. Two atom subsets (indicated for brevity with the curled brackets) consisting of all eight H-1 and all H-6 were defined for the calculation; the two curves report the distribution of distances among all the possible H-1/H-6 pairs (both intra- and inter-glycosidic) averaged over the MD run.

2.2. Molecular dynamics

The MD runs at 300 K unambiguously confirm that one A chain easily penetrates within the CD cavity with little changes of the macrocycle conformation. This result was obtained in all the runs starting from a conformation with a local energy minimum having all the alkyl/acyl chains outside the cavity (Fig. 5A). Even in this conformation the macrocycle is severely dis-

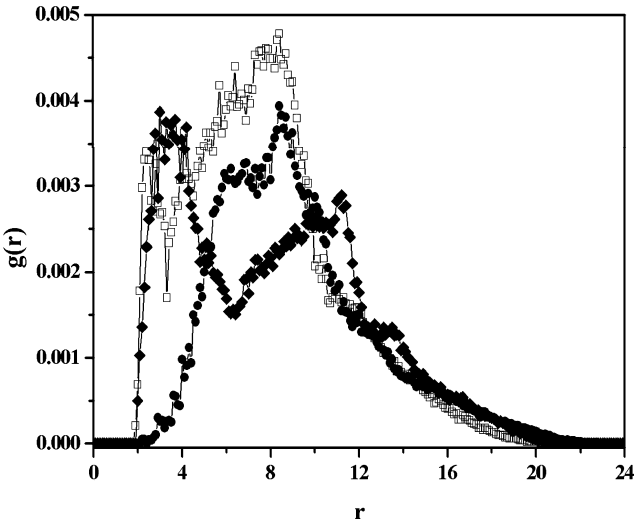

Fig. 4. Spherical radial distribution function $g(r)$ of the {H-3}–{A5} (empty squares), {H-4}–{A5} (filled circles) and {H-5}–{A5} (filled diamonds) distances r (Å) in **1**. The atom subsets are defined as in Fig. 3, and their distances are averaged as described in the same Figure.

torted from the characteristic cone shape of smaller membered CDs and native γCD, in keeping with the NMR results, while all the glucopyranose rings keep throughout their $^4C_1$ chair conformation. The insertion of one A chain is quite fast and always takes place within a few tens of ps, leading also to a significant decrease of the average potential energy by about 15 kcal mol^{-1}. Afterwards, this chain is strongly held in place within the cavity until the end of all dynamic runs, i.e., effectively for an overall time interval longer than 10 ns.

An extensive set of conformations periodically saved during the MD runs were also energy minimised in search of the global energy minimum. A total of 1250 geometries were considered, obtained in two different MD runs, which afforded a large collection of conformations, often having a similar energy. The structure corresponding to the lowest energy minimum is shown

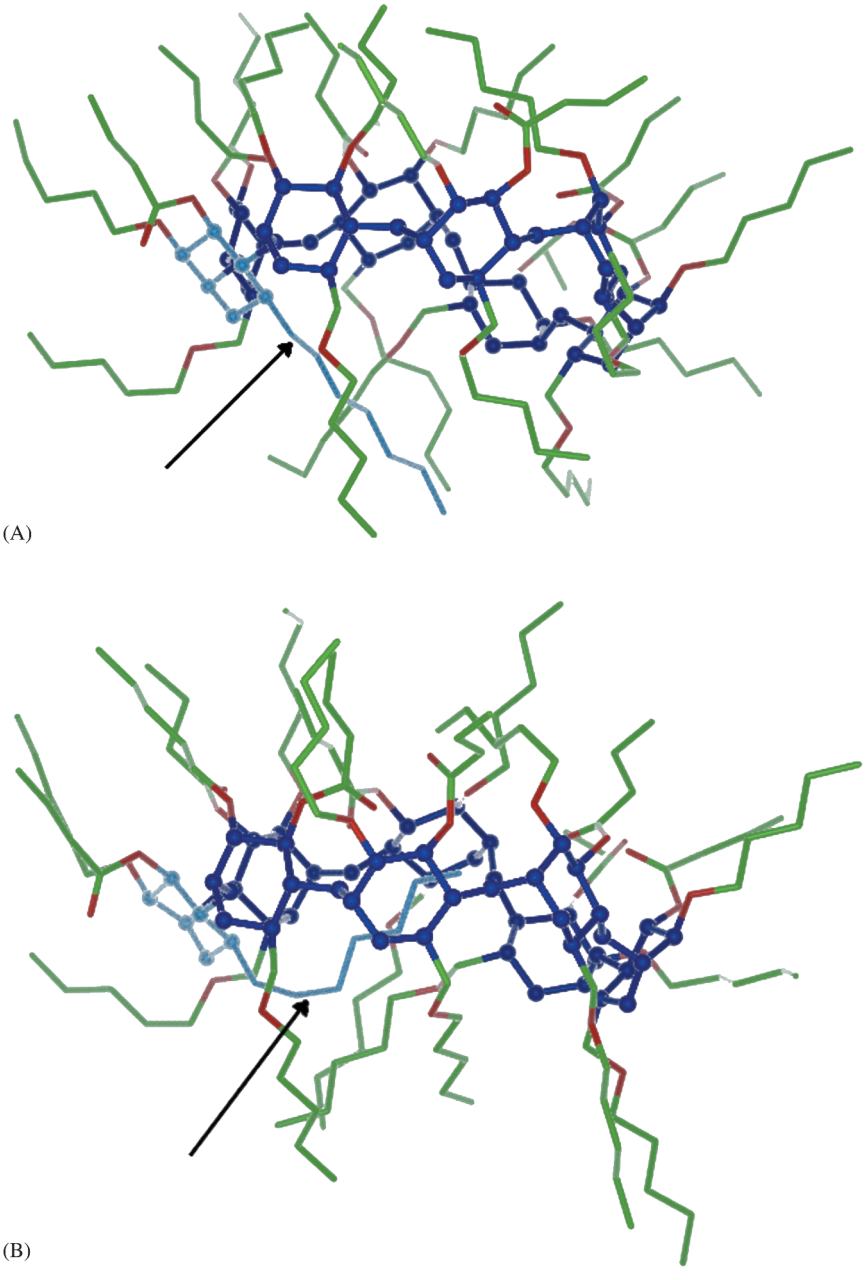

Fig. 5. A: The initial conformation of **1** with a local energy minimum showing no self inclusion. The alkyl/acyl chains are shown in green, with the oxygen atoms in brown, while the A chain that shall undergo self-inclusion (indicated with an arrow) is shown in pale blue together with its glucopyranose unit, while the other glucopyranose units forming the macrocycle are shown in dark blue. For clarity, the macrocycle is also displayed in balls and sticks. B: The most stable conformation of **1** with self inclusion of one A chain (indicated with an arrow).

in Fig. 5B, with the macrocycle drawn as a ball-and-stick structure. Its large deviations from the ideal cone shape geometry, similar to those before self-inclusion, are again evident. The energy of this conformation is lower by more than 15 kcal mol^{-1} than the local energy minimum before any inclusion takes place (Fig. 5A). As expected, this is roughly the decrease shown by the average potential energy in the MD runs.

It is noteworthy that in all the MD runs the chain never leaves the CD cavity, a feature suggesting a lack of microscopic reversibility on the time scale of the present simulations. The large number of degrees of freedom of this molecule, related both to the large number of atoms and to the flexibility of the alkyl/acyl chains, may explain such apparent irreversibility. In fact, the fluctuations in total energy are large enough to overcome the potential energy gain due to self-inclusion. However, the excess energy must be concentrated on the included arm, if it has to leave the cavity, whereas from a purely statistical viewpoint it is much more likely distributed at random among the various degrees of freedom. Moreover, this process requires a concerted motion of the trapped A chain out of the cavity and of the outer arms that must not obstruct its escape route. In fact, some alkyl/acyl chains do stretch above both rims so as to optimize their van der Waals interactions. In conclusion, the expulsion of the A arm from the cavity should eventually take place, but it is an entropically unlikely event that requires simulation times currently beyond computing possibilities. In this context, it is also interesting to note that also a B chain may show a fleeting inclusion at the beginning of some MD runs. However, this short-lived inclusion is not as deep within the cavity as for an A chain. In fact, a B chain, which is bound to the secondary rim, never approaches the opposite rim upon inclusion, unlike what happens to the included A chain whose terminal methyl group can get quite close to hydrogens H-3 and H-5, as shown by the ROE experiments and by the RDF curves of Fig. 4. Accordingly, the 'inclusion' of B chains is more related to their conformational freedom than to significant van der Waals interactions with the macrocycle. Thus, persistent self-inclusion of a B chain was never observed, while the self-inclusion of an A chain occurred in all the MD runs. Therefore, we conclude that the latter process is by far the preferred one.

The idea of native CDs, γCD among them, characterized by a rigid macrocycle, was recently questioned.[38] In the case of **1**, the presence of alkyl/acyl substituents decreases, to some extent, the macroring freedom of motion. This feature can be clearly detected by plotting the distances between pairs of glycosidic or pyranose ring oxygen atoms on opposite sides of the macrocycle (their topology is shown in Fig. 6) as a function of time. The former can be related to the macroring distortion from the ideal torus shape, and the latter to the glucose units tilting. Two such distances in **1** are shown in Fig. 7 for either pair of oxygens, corresponding to the

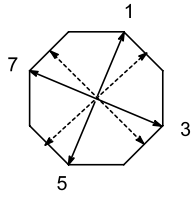

Fig. 6. Sketch of the macrocycle topology. The vertices correspond to the glycosidic oxygen atoms, while the individual rings are simply represented by segments. The double-headed solid arrows connect topologically opposite glycosidic oxygens (1-5 and 3-7, for instance), while the dashed arrows connect analogous pyranose ring oxygens.

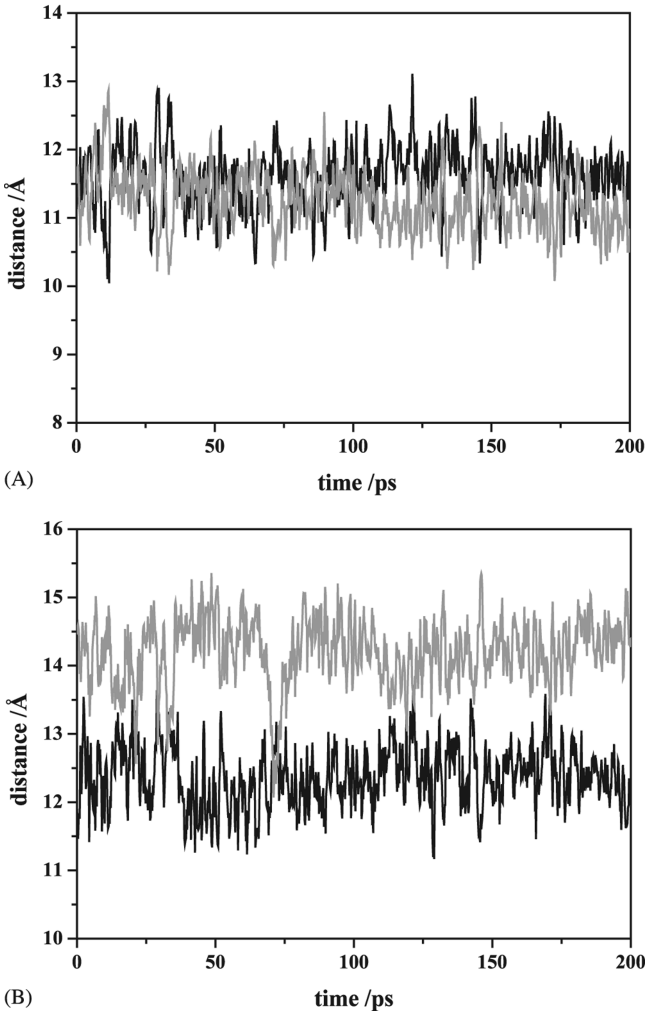

Fig. 7. The distances among selected oxygen atoms across the macrocycle plotted as a function of time during a 200 ps MD run for **1**. Panel A shows the distance between the glycosidic oxygens O-1–O-5 and O-3–O-7 (see Fig. 6), and panel B shows the distance between their adjacent pyranose ring oxygens (see Fig. 6). Note the relatively small fluctuation of these distances on the vertical axis compared to the corresponding ones in the native γCD (see Fig. 8).

non-bonded separations O(n)–O($n+4$), n indicating the position on the macrocycle. We chose for n the values 1 or 3 (see Fig. 6), so as to have a better picture of the overall macrocycle deformation. Both the amplitudes of the fluctuations and their characteristic times are important. Upon comparison with the corresponding plots for native γCD, reported in Fig. 8, we note that these fluctuations are severely damped in **1**, with a significantly smaller amplitude. The clear modulation of these fluctuations in native γCD for the distance between the glycosidic oxygen pairs should also be noted. At the same time, these fluctuations are slower in **1** than in native γCD, and take place with longer characteristic times, or equivalently with a lower frequency. This is best seen through the Fourier transforms of the plots in Figs. 7 and 8, shown in Fig. 9. In the case of native γCD, the most relevant feature consists of a twin peak centred at about 0.38–0.39 ps^{-1} in for the pyranose ring and glycosidic oxygens (for clarity, only the result for the former oxygens is reported). Additionally, we find a weaker peak at 0.17 ps^{-1} for the pyranose

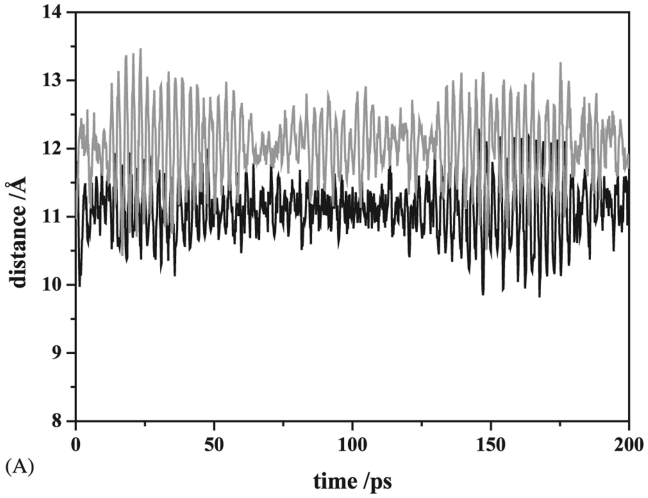

Fig. 8. The same as in Fig. 7 for the native γCD. Note on the vertical axis the larger fluctuation of these distances compared to the corresponding ones in **1** (see Fig. 7).

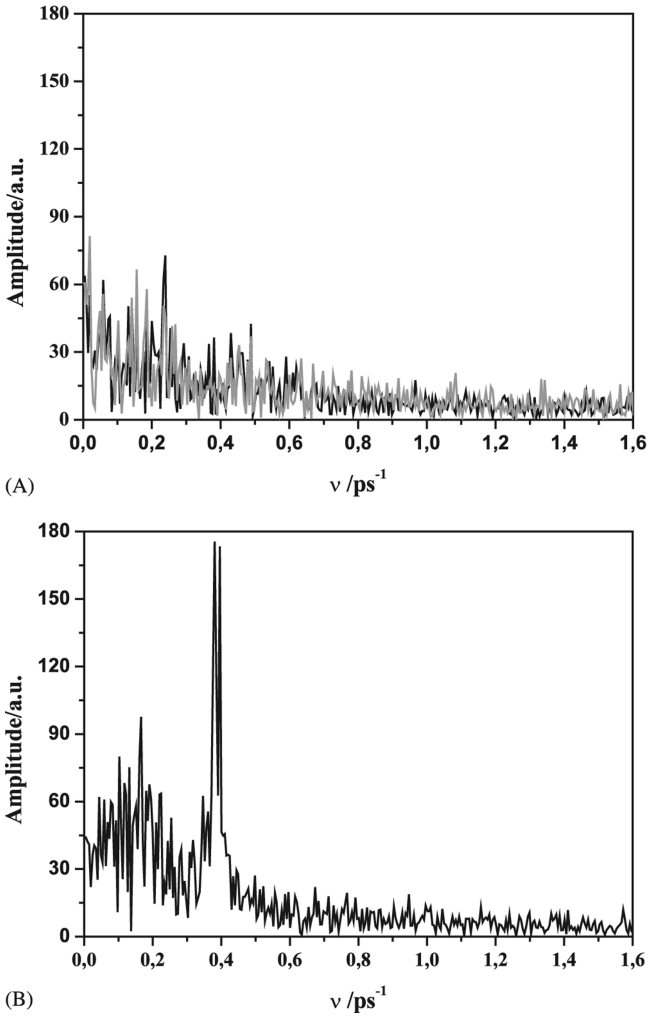

Fig. 9. The Fourier transform of the curves reported in Figs. 7 and 8. Panel A shows the results for the glycosidic oxygen atoms (black curve) and for the pyranose ring oxygen atoms (gray curve) of **1** (see also the text). Panel B reports the result for the pyranose ring oxygens of the native γCD. The analogous plot for the glycosidic oxygens shows only a twin peak at 0.38–0.39 ps^{-1}, and is not reported for clarity.

ring oxygens, superimposed to a broad distribution of frequencies suggesting a rather noisy and chaotic dynamics of the macrocycle. In **1** no major peak is found, and the intramolecular dynamics is characterized by a broad distribution of low-frequency peaks, the larger ones being found at 0.23 ps^{-1} and at 0.16 ps^{-1} for both the pyranose ring and the glycosidic oxygens, even though with different heights. As a further point of interest, it can easily be noted by visual inspection of Fig. 7 (upper panel) that in **1** the motion of the 1-5 glycosidic oxygen pair is essentially anticorrelated with that of the 3-7 pair (see Fig. 6), implying that the macrocycle undergoes a 'breathing' motion with ellipsoidal deformations along orthogonal directions. Such anticorrelation is basically absent in native γCD. Furthermore, both molecules display a weaker anticorrela-

tion on the distance of the pyranose ring oxygens, due to a tilting motion of the glycosidic rings superimposed to the breathing motion of the macrocycle.

The side chains of **1** show the expected large flexibility, sweeping a relatively large area above the two rims. This flexibility is mainly related to the length of the chains, but it is also affected by the nature of the group connecting them to either rim (i.e., ether linkage versus ester). A useful way to quantify the chain mobility consists on the analysis of the minimum root-mean-square distances between the atoms of a given chain (i.e., the A, B or C chains) in all the pairs of the different conformations encountered during a long MD run (5 ns, sampled every 10 ps). It turns out that the A chains are the most mobile ones, easily exploring regions separated on the average by more than 3 Å, even though one of them is trapped within the CD cavity during most part of the simulation. It should be added anyway that such arm is by no means frozen, but rather it is wandering about within the cavity. The B chain is slightly more constrained and never undergoes genuine self-inclusion, whereas the C chains are by far the less mobile ones, the amplitude of their motion never exceeding the range of about 1.5–2 Å. The lower mobility of the latter chains can be explained both through their shorter length and greater rigidity of its ester groups (whose stiff U-shaped conformation is retained during the whole dynamics) bound to the CD macrocycle. The mobility and the interactions of the side chains strongly affect also the dynamics of the macrocycle. In fact, they slow down the macrocycle dynamics at room temperature compared to native γCD in spite of the lack of the hydrogen-bond network. We attribute this effect to the friction among the alkyl side chains, an effect that should be absent with short alkyl substituents, such as CH_3 groups in permethylated cyclodextrins. Accordingly, **1** lacks the characteristic frequency at 0.38–0.39 ps^{-1} (see the plots in Fig. 9), and shows only lower frequency motions.

Finally, we explored the possibility of a simultaneous inclusion of two different A chains within the cavity. Thus, we took the minimum-energy conformation with self-inclusion of one A chain and tried to insert a second A chain bound on the opposite side of the macrocycle by appropriate changes of the relevant torsion angles. A simple energy minimization showed that upon such double self-inclusion **1** has roughly the same energy as the conformation with no self-inclusion whatsoever. However, during a subsequent MD run one of the included chains is almost immediately expelled from the cavity, thus yielding again a single self-included chain. This result shows that this is not a favourable conformation, both for energetic and entropic reasons.

In conclusion, NMR and MD data point out three major geometrical features of **1**: (*i*) the macrocycle displays a geometry far from the symmetrical torus shape usually reported for native cyclodextrins (although an average C_8 symmetry is retained on the NMR timescale); (*ii*) the lipophilic alkyl/acyl tails interact with the cavity, and self-inclusion of one 6-*O*-pentyl chain takes place; (*iii*) the amplitude of macroring motion in **1** is less than in native γCD. To summarize, because of the interactions among the alkyl chains **1** shows a larger equilibrium deformation of the macrocycle from the idealized geometry than native γCD, but at the same time it displays both smaller amplitude and lower frequency shape fluctuations.

These findings add new motives for the formulation of a model for binding, recognition and chiral discrimination of guest molecules in the presence of **1**, as recently postulated in the case of complexes with (*R*)- and (*S*)-enflurane.[39]

3. Experimental

3.1. Synthesis and NMR spectroscopy

Cyclohexane-d_{12} was purchased from Aldrich Chemical Co. (Milano, Italy). Synthesis and purification of octakis(3-*O*-butanoyl-2,6-di-*O*-pentyl)-γ-cyclodextrin (Lipodex E, **1**), together with a more recent improved procedure, has been described elsewhere.[1,2] NMR experiments were carried out on a Bruker ARX 400 and Avance 500 machines, working at the operating frequencies of 400 and 500 MHz for ^1H. All chemical shifts are referenced to Me_4Si. The assignment of the ^1H NMR spectrum of **1** was supported by two-dimensional double quantum filtered COSY (DQF-COSY) and homonuclear Hartman–Hahn correlation (HOHAHA) experiments. General settings for homonuclear 2D NMR experiments: 2 K points in F2, 512 increments in F1, 3 s recycling delay, zero filling to 2 K before Fourier transform, mixing time for HOHAHA transfer ranging from 50 to 200 ms. Two-dimensional correlation experiments via dipolar coupling in the rotating frame (ROESY) were performed by using the pulse sequence proposed by Desvaux et al.[40] for off-resonance ROESY with adiabatic rotation in order to minimise artefacts due to homonuclear Hartmann–Hahn magnetisation transfer, improve peak shape and sensitivity. Several values of the tilt angle $\theta = \arctan[(\gamma B_1/2\pi)/\Delta]$, with Δ = distance between the spin-lock field frequency and the central frequency of the spectrum, were tested ($\theta = 78°, 70°, 55°, 40°$). The results reported in the text are referred to $\theta = 40°$. In these conditions only H-4–H-5 cross-peak resulted in phase with diagonal, thus affected by HOHAHA transfer. ^{13}C spectral assignments were confirmed by reverse detection C–H correlation experiments (HMQC). Self-aggregation phenomena (see Section 2.1) were minimized by

using dilute soln (5 mM). The molecular weight, determined from a cyclohexane soln, was consistent with monomeric **1** (m/z 3005.8, $[M + Na]^+$).[41]

3.2. MD simulations

3.2.1. Numerical procedure. All simulations were performed with the InsightII/Discover 2000 package, distributed by Molecular Simulations Inc. (San Diego, USA)[42], (now Accelrys) using the consistent valence force field[43] CVFF with a Morse potential for the bonded atoms. The input geometry was generated from scratch by using the available library fragments and fully minimized up to an energy gradient lower than 10^{-3} kcal mol^{-1} Å^{-1}. In this geometry, corresponding to a local energy minimum, all the alkyl/acyl substituents stayed outside the molecular cavity as initially drawn. MD simulations were performed in vacuo with a dielectric constant $\varepsilon = 1$ and at a constant temperature ($T = 300$ K), controlled through the Berendsen thermostat, and the integration of the dynamical equation was carried out using the Verlet algorithm with a timestep of 1 fs. After an initial equilibration run of 10 ps, the data collection was carried out by running the MD simulations for different time intervals. Two long runs each lasting for 5 ns and additional shorter runs lasting for 200 ps unambiguously established the favourable and systematic self-inclusion of one A chain. An extensive set of molecular geometries were periodically saved and fully minimized up to a gradient of less than 10^{-3} kcal mol^{-1} Å^{-1}.

3.2.2. Data analysis. The geometries encountered during the dynamic runs can be usefully analysed through the RDF plots. The radial distribution function $g_{ij}(r)$ yields the probability density of finding atoms j at a distance r from atoms i. In the present case, namely for an isolated system in vacuo, it is defined as

$$g_{ij}(r) = \frac{d\langle N_{ij}(r)\rangle}{dV(r)}$$

where $d\langle N_{ij}(r)\rangle$ is the average number of times the j atoms are comprised in a spherical shell of thickness dr at a distance r from atoms i within an MD run. Thus, $g_{ij}(r)$ also yields the average local density of atoms j in the shell volume $dV(r)$ comprised at a distance between r and $r + dr$ from atoms i.

Acknowledgements

The authors wish to thank Professor Dr M. Morbidelli, both ETH Zürich and Politecnico di Milano, for his continuous support that made this collaboration possible. V.S. thanks the Fonds der Chemischen Industrie for financial support.

References

1. König, W. A.; Krebber, R.; Mischnick, P. *J. High Resolut. Chromatogr.* **1989**, *12*, 732–738.
2. Juza, M.; Di Giovanni, O.; Biressi, G.; Schurig, V.; Mazzotti, M.; Morbidelli, M. *J. Chromatogr. A* **1998**, *813*, 333–347.
3. König, W. A. *J. High Resolut. Chromatogr.* **1993**, *16*, 569–586.
4. Juza, M.; Braun, E.; Schurig, V. *J. Chromatogr. A* **1997**, *769*, 119–127.
5. Biressi, G.; Quattrini, F.; Juza, M.; Mazzotti, M.; Schurig, V.; Morbidelli, M. *Chem. Eng. Sci.* **2000**, *55*, 4537–4547.
6. Schurig, V. *J. Chromatogr. A* **1994**, *666*, 111–129.
7. Schneider, M.; Ballschmiter, K. *Chem. Eur. J.* **1996**, *2*, 539–544.
8. Schneider, M.; Ballschmiter, K. *J. Chromatogr. A* **1999**, *852*, 525–534.
9. Schurig, V.; Juza, M. *J. Chromatogr. A* **1997**, *757*, 119–135.
10. Snopek, J.; Smolková-Keulemansová, E.; Cserháti, T.; Gahm, K. H.; Stalcup, A. Cyclodextrin in Analytical Separation Methods. In *Comprehensive Supramolecular Chemistry*, Atwood, J. L.; Davies, J. E. D.; Macnicol, D. D.; Vögtle, F. Exec. Eds.; Pergamon Press: Oxford, 1996; Vol. 3, Szejtli, J.; Osa, T. Vol. Eds.; pp. 516–571.
11. Berthod, A.; Li, W.; Armstrong, D. W. *Anal. Chem.* **1992**, *64*, 873–879.
12. Bradshaw, J. S.; Chen, Z.; Yi, G.; Rossiter, B. E.; Malik, A.; Pyo, D.; Yun, H.; Black, D. R.; Zimmermann, S. S.; Lee, M. L.; Tong, W.; D'Souza, V. T. *Anal. Chem.* **1995**, *67*, 4437–4439.
13. Uccello-Barretta, G.; Balzano, F.; Caporusso, A. M.; Iodice, A.; Salvadori, P. *J. Org. Chem.* **1995**, *60*, 2227–2231.
14. Lipkowitz, K. B. *Chem. Rev.* **1998**, *98*, 1829–1873.
15. Lipkowitz, K. B.; Pearl, G.; Coner, B.; Paterson, M. A. *J. Am. Chem. Soc.* **1997**, *119*, 600–610.
16. Lipkowitz, K. B.; Coner, B.; Paterson, M. A. *J. Am. Chem. Soc.* **1997**, *119*, 11269–11276.
17. Lipkowitz, K. B.; Coner, B.; Paterson, M. A.; Morreale, A.; Shackelford, J. *J. Org. Chem.* **1998**, *63*, 732–745.
18. Beier, T.; Höltje, H.-D. *J. Chromatogr. B* **1998**, *708*, 1–20.
19. Immel, S. In *Cyclodextrin: From Basic Research to Market, Proceedings of the 10th International Cyclodextrin Symposium*, Szejtli, J., Ed.; Waker Biochem. Corp., Adrian, 2000; pp 24–31.
20. Koshland, D. E. *Angew. Chem., Int. Ed. Engl.* **1994**, *33*, 2375–2378.
21. Lichtenthaler, F. W. *Angew. Chem., Int. Ed. Engl.* **1994**, *33*, 2364–2374.
22. Schneider, H.-J.; Hacket, F.; Rüdiger, V. *Chem. Rev.* **1998**, *98*, 1755–1785.
23. See Table 2 of Ref. 22 and references therein.
24. Bates, P. S.; Parker, D.; Patti, A. F. *J. Chem. Soc., Perkin Trans. 2* **1994**, 657–668.
25. Botsi, A.; Yannakopoulou, K.; Hadjoudis, E.; Perly, B. *Magn. Reson. Chem.* **1996**, *34*, 419–423.
26. Inoue, Y. *Annu. Rep. NMR Spectrosc.* **1993**, *27*, 60–101.
27. Jacob, J.; Geßler, K.; Hoffmann, D.; Sanbe, H.; Koizumi, K.; Smith, S. M.; Takaha, T.; Saenger, W. *Angew. Chem., Int. Ed. Engl.* **1998**, *37*, 605–609.
28. Endo, T.; Nagase, H.; Ueda, H.; Shigihara, A.; Kobayashi, S.; Nagai, T. *Chem. Pharm. Bull.* **1997**, *45*, 1856–1859.

29. Harata, K. *Chem. Rev.* **1998**, *98*, 1803–1827.
30. Uccello-Barretta, G.; Balzano, F.; Cuzzola, A.; Menicagli, R.; Salvadori, P. *Eur. J. Org. Chem.* **2000**, 449–454.
31. Neuhaus, D.; Williamson, M. *The Nuclear Overhauser Effect in Structural and Conformational Analysis*; VCH Publishers: New York, 1989; pp 318–323.
32. Jullien, L.; Canceill, J.; Lacombe, L.; Lehn, J.-M. *J. Chem. Soc., Perkin Trans. 2* **1994**, 989–1002.
33. Ikeda, H.; Nakamura, N.; Ise, N.; Oguma, N.; Nakamura, A.; Ikeda, T.; Toda, F.; Ueno, A. *J. Am. Chem. Soc.* **1996**, *118*, 10980–10988.
34. Uccello-Barretta, G.; Cuzzola, A.; Balzano, F.; Menicagli, R.; Iuliano, A.; Salvadori, P. *J. Org. Chem.* **1997**, *62*, 827–835.
35. Kawabara, T.; Takamura, M.; Matsushita, A.; Ikeda, H.; Nakamura, A.; Ueno, A.; Toda, F. *J. Org. Chem.* **1998**, *63*, 8729–8735.
36. Köhler, J. E. H.; Hohla, M.; Richters, M.; König, W. A. *Chem. Ber.* **1994**, *127*, 119–126.
37. Dodziuk, H.; Chmurski, K.; Jurczac, J.; Koźmiński, W.; Lukin, O.; Sitkowski, J.; Stefaniak, L. *J. Mol. Struct.* **2000**, *519*, 33–36.
38. Dodziuk, H. *Introduction to Supramolecular Chemistry*; Kluwer: Dordrecht, 2002, Chapter 7.4, pp 207–219.
39. Mele, A.; Raffaini, G.; Juza, M.; Schurig, V. In *Cyclodextrin*: *From Basic Research to Market*, *Proceedings of the* 10*th International Cyclodextrin Symposium*; Szejtli, J., Ed.; Waker Biochem. Corp: Adrian, 2000; pp 114–121.
40. Desvaux, H.; Berthault, P.; Birlirakis, N.; Goldman, M.; Piotto, M. *J. Magn. Reson. A* **1995**, *113*, 47–52.
41. Mele, A.; Malpezzi, L. *J. Am. Soc. Mass Spectrom.* **2000**, *11*, 228–236.
42. Accelrys Inc., InsightII 2000, San Diego, 2000. See also the URL http://www.accelrys.com.
43. Dauber-Osguthorpe, P.; Roberts, V. A.; Osguthorpe, D. J.; Wolff, J.; Genest, M.; Hagler, A. T. *Proteins: Structure, Function and Genetics* **1988**, *4*, 31–47.